

Automatic Quantification of Ejection Fraction from Gated Myocardial Perfusion SPECT

Guido Germano, Hosen Kiat, Paul B. Kavanagh, Mady Moriel, Marco Mazzanti, Hsiao-Te Su, Kenneth F. Van Train and Daniel S. Berman

Department of Medical Physics and Imaging, Division of Nuclear Medicine, Department of Imaging and Division of Cardiology, Department of Medicine, Cedars-Sinai Research Institute, Cedars-Sinai Medical Center, Los Angeles, California; and Department of Radiological Sciences and Department of Medicine, UCLA School of Medicine, Los Angeles, California

We have developed a completely automatic algorithm to quantitatively measure left ventricular ejection fraction (LVEF) from gated ^{99m}Tc -sestamibi myocardial perfusion SPECT images.

Methods: The algorithm operates in the three-dimensional space and uses gated short-axis image volumes. It segments the left ventricle (LV), estimates and displays endocardial and epicardial surfaces for all gating intervals in the cardiac cycle, calculates the relative left ventricular cavity volumes and derives the global EF from the end-diastolic and end-systolic volume, all without operator interaction. The algorithm for measuring LVEF was tested in 65 clinical patients undergoing 16-interval and 8-interval rest-gated SPECT and validated against first-pass radionuclide ventriculography. **Results:** Automatic segmentation and contouring of the LV was successful in 65/65 (100%) of the studies. Agreement between EFs measured from 8-interval gated SPECT and EFs calculated from first-pass data was high ($y = 2.44 + 1.03x$, $r = 0.909$, $p < 0.001$, $\text{s.e.e.} = 6.87$). Agreement between EF values measured from 16-interval and 8-interval gated SPECT was excellent ($y = -2.7 + 0.97x$, $r = 0.988$, $p < 0.001$, $\text{s.e.e.} = 2.65$), the latter being on average lower by 3.71 percentage points. **Conclusion:** Our automatic method is rapid and highly agrees with conventional radionuclide measurements of EF, thus providing clinically useful additional information to complement myocardial perfusion studies.

Key Words: automatic ejection fraction quantitation; technetium-99m-sestamibi; myocardial perfusion imaging; single-photon emission computed tomography

J Nucl Med 1995; 36:2138-2147

Technetium-99m-sestamibi is widely used in myocardial perfusion SPECT imaging, as it offers the advantages of higher photon energy and higher injectable dose compared to ^{201}Tl (1-2). The high counting statistics of ^{99m}Tc -sestamibi have favored its use in connection with electrocardiographic (EKG) gating. In gated perfusion SPECT proto-

cols, several perfusion image sets (typically 8 or 16) corresponding to different phases (intervals, frames, gates) of the cardiac cycle are acquired (3-4). Image sets corresponding to the diastolic portion of the cardiac cycle may be summed together to create systole-deleted images, thereby avoiding the blurring inherent in combining systolic and diastolic data (4), as well as artifacts resulting from segmental contraction heterogeneity (5). Summing all the projection images corresponding to the individual intervals before reconstruction is equivalent to acquiring a static perfusion SPECT study and results in what are generally referred to as ungated or summed images.

Reconstructing each interval of a gated perfusion SPECT study into a tomographic image set allows visual (6) or quantitative (7-11) estimation of functional parameters such as myocardial motion and thickening, as is also done with gated PET (12,13). In addition, gating helps identify artifacts caused by tissue attenuation (14,15). Assessment of the variation of the left ventricular cavity volume between diastole and systole is extremely important, as it allows calculation of the left ventricular ejection fraction (LVEF), a fundamental diagnostic and prognostic predictor of coronary artery disease (16-20). Ejection fractions have been traditionally estimated from either planar (21-24) or SPECT (10,25-28) gated blood-pool studies; however, blood-pool studies cannot provide simultaneous information on myocardial function and perfusion and therefore cannot obviate the need for a separate rest study in patients without prior myocardial infarction (6). Unlike myocardial motion and thickening, LVEFs are difficult to estimate visually because they are derived quantities. In gated blood-pool studies, ejection fractions are derived as ratios of left ventricular cavity counts or volumes at end-diastole and end-systole. In gated perfusion studies, there is no activity in the blood pool, and ejection fractions can only be derived from the left ventricular cavity volumes EDV (at end-diastole) and ESV (at end-systole)

Received Dec. 19, 1994; revision accepted Apr. 12, 1995.
For correspondence or reprints contact: Guido Germano, PhD, Director, Nuclear Medicine Physics, Cedars-Sinai Medical Center A047 N, 8700 Beverly Blvd., Los Angeles, CA 90048.

$$\text{EF} = \frac{\text{EDV} - \text{ESV}}{\text{EDV}} \times 100. \quad \text{Eq. 1}$$

Determination of the left ventricular cavity volume (also referred to as endocardial volume) implies outlining of the corresponding endocardial surface. It has been suggested that endocardial contours could be manually traced on a midventricular horizontal long-axis and vertical long-axis slice of the left ventricle using a threshold equal to 34% of the maximal myocardial counts, and the global endocardial volume can be estimated from geometric considerations using the Sandler and Dodge assumption (15,22). Since this method is manual, it is susceptible to error and poor reproducibility, especially when severe perfusion defects are present. In addition, practical processing considerations require the drawing of contours in only two images per phase, imposing the constraint that the endocardial geometry be perfectly ellipsoidal and utilizing only a bi-planar portion of the full three-dimensional tomographic image. A modification of this technique has been proposed in which the endocardial borders would be determined semi-automatically from a larger number of long-axis slices (29), although the algorithm has not yet been applied to gated studies. Automatic determination of the endocardial surface of the left ventricle has been sought by Faber et al. using a combination of: (a) image intensity gradients calculation for the initial estimate of the surface and (b) iterative relaxation labeling for surface refinement (10). In this implementation, the long-axis of the left ventricle must be manually drawn on a user-selected midmyocardial image. The location and length of the long-axis specifies the location and orientation of the valve plane as well as the parameters of the coordinate system used in the analysis. In addition, if the method's assumption that the myocardium has higher counts than the surrounding structures is correct, accurate tracement of the long-axis is key to isolating the left ventricle for surface extraction purposes. Drawbacks of this method include the dependence on a manual operator for segmentation, valve plane and search limits definition, its unknown efficacy when spurious hot structures, such as the liver, spleen or intestine, are present in the proximity of the heart and the possibility that the relaxation labeling process may not converge (10,30–31).

We have developed a totally automatic method to determine global ejection fractions from gated myocardial perfusion SPECT, optimized its parameters using phantom data and validated it in a large ($n = 65$) patient population against the standard resting first-pass planar technique. The method requires as input the gated short-axis image sets and accomplishes the tasks of left ventricle segmentation, valve plane, endocardial and epicardial surfaces determination and ejection fraction calculation entirely without operator interaction. Its ease of use, fast execution (<30 sec) and portability throughout the Unix environment without need for proprietary hardware make this method a substantial improvement on previous approaches and has the potential to further promote the use of gated SPECT in the clinical practice of nuclear cardiology.

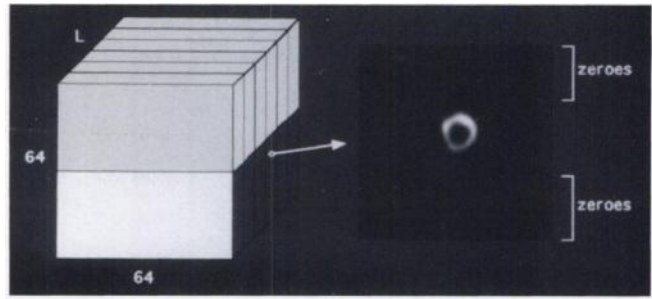


FIGURE 1. Automatic segmentation of left ventricular myocardium. The initial threshold used in the clusterification process is based on the maximal count activity in the upper half of the transaxial image volume, i.e., the area that should contain at least part of the heart if the study has been correctly reconstructed and reoriented. When present, hepatic activity is generally confined to the lower left quadrant of the short-axis image volume, while splenic or intestinal activity is likely to appear in the lower right quadrant.

THEORY

Left Ventricular Segmentation

The gated SPECT ejection fraction quantification algorithm starts by segmenting the left ventricle. The maximal voxel count value C_{max} in the upper half (Fig. 1) of the ungated $64 \times 64 \times L$ ($L < 64$) short-axis image volume is calculated. If the study has been correctly acquired and reconstructed, that regional maximum is likely to correspond to the myocardium. Since the transaxial reconstruction process is limited to the portion of the projection image set that contains the left ventricle, the uppermost (Z_u) and lowermost (Z_l) portion of the short-axis image volume will consist of zeroed pixels (Fig. 1). The segmentation algorithm sets all Z_l pixels to C_{max} to connect and increase the apparent size of truncated structures below the left ventricle. The entire image volume is then thresholded to 50% of C_{max} , binarized and the binary clusters in the volume determined. Each cluster, or set of connected voxels, is constructed by depth-first search (32) from a seed voxel (the first nonzero voxel encountered while scanning the short-axis volume from one of its corners). Once a cluster has been identified its location is marked, its voxels are zeroed and the algorithm continues. When all clusters have been determined, those physiologically too small (<50 ml) to represent the left ventricular myocardium are eliminated. For each remaining cluster, the smallest rectangle that circumscribes it in every short-axis slice is determined. If only one cluster remains and the absolute length difference between the sides of its bounding rectangle is less than 1 cm, the cluster is assumed to correctly identify the left ventricular myocardium. If two or more clusters remain (suggesting that thresholding was successful in separating the left ventricle from other hot structures), the one closest to the center of the upper right quadrant of the short-axis image volume is chosen.

In either case, if the absolute length difference between the sides of its bounding rectangle is more than 1 cm (suggesting that spurious hepatic or intestinal activity is still connected to that in the left ventricle, erosion of the cluster is performed by raising the threshold in 5% steps from the original value of $C_{max}/2$ until the cluster is broken into two or more pieces. The two larger subclusters are selected and assigned to the liver and the LV myocardium (again, based on likely location considerations). Then, dilation of both clusters is performed by iteratively adding 1-voxel wide layers of voxels, checking every voxel in each layer to ensure that its addition will not reconnect the clusters or make the absolute

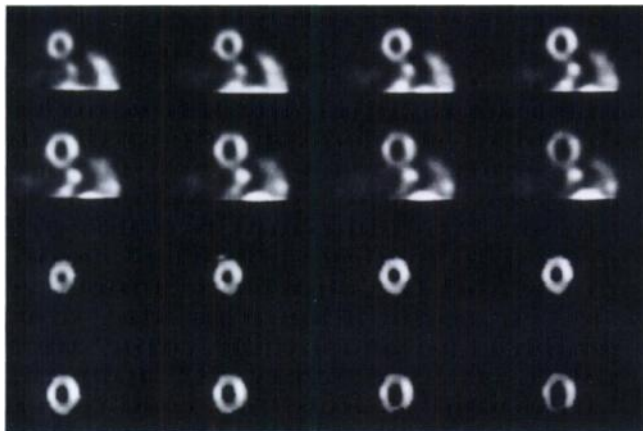


FIGURE 2. Thresholding, clusterification and rule-based cluster selection and refinement by eroding/dilating techniques generate a binary mask from the original short-axis image volume (top two rows). Multiplying the mask by the original image isolates the left ventricular myocardium (bottom two rows).

length difference between the sides of the bounding rectangle larger than 1 cm. Dilation is continued until the original $C_{max}/2$ threshold is reached. The binary cluster representing the left ventricle is used as a mask in the subsequent phases of the algorithm. An example of the segmentation for a patient study with considerable hepatic and intestinal uptake is shown in Figure 2.

The aforementioned segmentation algorithm is enhanced further by the use of a Hough transform extension when any of the following conditions is true: (a) segmentation returns a null cluster, (b) the liver cluster's axial coordinate is superior to that of the left ventricular cluster or (c) the volume of the smallest parallel piped circumscribing the left ventricular cluster is much larger (>1000 ml) than the expected volume of the left ventricle. In those cases, all the short-axis slices, S_i , are multiplied by a weight factor and summed to produce a single slice S . The weight for slice S_i is defined as:

$$w_i = 1 - 2 \left| \frac{i - \frac{N}{2}}{N} \right|, \quad \text{Eq. 2}$$

where N is the total number of short-axis slices. In other words, middle slices have a greater weight because they are more likely to contain the left ventricle. The local maxima in the summed slice S are identified as pixels containing counts above a certain threshold and greater than their four immediately neighboring pixels (NSEW).

The classical Hough transform is applied to detect contiguous local maxima forming approximate circles (33). Each circle is assigned a score proportional to the average count value along its circumference and the ratio of that value to the average count at the center, so as to favor doughnut-like count distributions. The circle with the highest score is deemed the most likely to represent the left ventricle and is expanded by 2 pixels outwards. For three-dimensional short-axis volumes, all voxels outside the cylinder with that circle for section are discarded. A 50% threshold is applied to voxels inside the cylinder, and voxels above the threshold are returned as the left ventricular mask. All parameters, rules and criteria used by the segmentation algorithm had been empirically determined previously from 40 static SPECT studies involving patients other than those described in this work.

Generation of Myocardial Surfaces and Volume/EF Measurement

The center of mass (COM) of the three-dimensional binary mask segmenting the left ventricular myocardium is chosen as the origin of the sampling coordinate system. If segmentation of the left ventricle was successful, the COM will be located within the left ventricular cavity, even in the presence of large perfusion defects. Radial count profiles originating from the COM are generated to achieve spherical sampling of the product of the binary mask and the short-axis image volume. The locus of the profiles' first maxima identifies the maximal count myocardial surface, which is an acceptable proxy for the midmyocardial surface. Sampling is done every 10° longitudinally (18 total) and every 10° latitudinally (36 total), resulting in 684 count profiles. It should be noted that a variable, potentially large number of these profiles is uniformly zero. In fact, both the basal portion of the myocardium at the valve plane and all perfusion defects will correspond to holes in the mask for which no maxima are returned. A fit of the midmyocardial surface to an ellipsoid is performed as reported by Germano et al. (34). The surface extraction process is then repeated using a new origin for the sampling coordinate system, which is determined as the projection of the original COM onto the ellipsoid's long-axis. This approach seeks to obviate errors in midmyocardial surface extraction, especially in cases where the original COM is close to the wall due to extensive perfusion defects. The process is iterated until the long-axis angular variation is less than 0.5° , which generally requires two to three iterations.

We now have an estimate of the midmyocardial surface containing perfusion holes, plus the ellipsoid that best fits it. To incorporate perfusion data from underperfused areas into the fit (fill the holes), a set of myocardial likelihood profiles (32 longitudinally and 24 latitudinally) is generated by extracting, from the unmasked and nonthresholded image, count profiles normal to the ellipsoid and convolving them with a feature detector consisting of the double derivative of a Gaussian with a s.d. $\sigma = 10$ mm.

$$-\frac{x^2}{2\sigma^2} - Ke(x^2 - \sigma^2). \quad \text{Eq. 3}$$

The local maxima of these profiles are extracted (there is generally at least one local maximum per profile). The final summed midmyocardial surface is then defined as that set of surface points, one per profile, which minimizes the sum of the cost of each surface point. The cost of each surface point is defined as a weighted sum of: (a) the deviation between its surface normal and corresponding ellipsoidal normal and (b) a nonlinear function of its distance from, and the magnitude of, each of the local maxima of the likelihood profile. An ellipsoid is finally fitted to this myocardial surface and will provide a sampling basis for processing the individual intervals. The sampling grid from which the ellipsoidal normals subtend is defined as the intersections of the 24 latitudes coplanar with and the 32 longitudes perpendicular to its long-axis.

For each interval (unmasked, unthresholded images), count profiles normal to the ellipsoid (24 latitudinally, 32 longitudinally) are extracted as done for the summed image. Then, as for the summed image, the profiles are convolved with the feature detector in Equation 3, the local maxima labeled and the myocardial surfaces corresponding to each interval defined. Temporal continuity is imposed as an additional constraint (i.e., homologous

points in adjacent intervals are penalized in proportion to their separation).

Having found the midmyocardial surfaces for every interval, we used the geometry of the end-diastolic surface, onto which is mapped the count distribution averaged over all intervals, to determine the valve plane. We took a 25% threshold of those counts, then fit a plane to the set of surface points lying on the boundary of the largest and most basal contiguous subthreshold area. This fit minimizes a cost equal to the weighted sum of the plane normal's deviation from a preferred direction and the sum of the distances from the plane to each boundary point, with distances from points apical to the plane constrained to ≤ 20 mm. The area of the surface points below threshold and basal to the valve plane is calculated; if lower than 10% of the total midmyocardial surface area, the threshold is iteratively raised and the process repeated. The valve plane in the end-diastole interval defines the myocardium as the collection of surface points derived from the ellipsoidal sampling normals apical to the plane; the same normals are assumed to define the myocardium in all other intervals. As the boundary points move, the valve plane also moves throughout the cardiac cycle.

For each interval, additional count profiles normal to and extending 20 mm in both directions from the midmyocardial surface are extracted. An asymmetric Gaussian is fitted to each profile and the inner ($s.d._{in}$) and outer ($s.d._{out}$) standard deviations of the Gaussian noted (35). The s.d.s measured from count profiles with peaks falling below 50% of the maximal myocardial count in that interval are labeled as invalid and replaced with s.d.s that minimize the sum of the absolute differences between each invalid s.d. and the s.d. of each of its four spatial neighbors. For each profile, an endocardial and an epicardial surface point are defined as those points lying a given percent of $s.d._{in}$ inward and a given percent of $s.d._{out}$ outward from the midmyocardial surface along its normal, respectively. Since the s.d.'s are expected to be greater in systole than in diastole if thickening occurs (36), the use of the same fractions of $s.d._{in}$ and $s.d._{out}$ for all intervals causes the endocardial and epicardial surface to thicken in a physiologic way from diastole to systole. To correct for partial volume, the effect of background activity and other sources of error, the endocardial and epicardial surfaces obtained for all intervals but end-diastole are further refined by imposing the anatomic constraint of the constant myocardial volume throughout the cardiac cycle. The myocardial volume is calculated as the difference between the epicardial volume (bound by the epicardial surface and the valve plane) and the endocardial volume (bound by the epicardial surface and the valve plane). The endocardial volumes, EDV (at end-diastole) and ESV (at end-systole), are also used to calculate the global LVEF, as in Equation 1.

The entire process, from left ventricular segmentation to ejection fraction calculation, requires less than 30 sec per 8-interval study on a Sun SPARC IPX computer using a X-Windows-based graphical user interface. When applied to nongated images, the algorithm returns endocardial and epicardial surfaces and their associated volumes in less than 4 sec.

METHODS

Phantom Experiments

To evaluate the influence of $s.d._{in}$ on the endocardial volumes used in the automatic algorithm's ejection fraction calculation, a chest phantom was imaged with a triple-detector camera. The phantom's myocardium (125 ml) contained 400 μ Ci 99m Tc and

TABLE 1
Patient Characteristics

Age (yr)	64 \pm 13 (31–83)
Sex (M/F)	45/20
Weight (lb)	185 \pm 42 (116–300)
Prior MI	25
Anterior	8 (4 large)
Inferior	12 (2 large)
Combined	3 (3 large)
Undetermined	2

bounded a known endocardial volume (63 ml). The acquisition was performed with LEHR collimation, continuous detector rotation, 3° projections and 20 sec of data collection per projection. The projection data were prefiltered with the standard two-dimensional Butterworth filter used in clinical practice for static 99m Tc-sestamibi SPECT (order = 2.5, critical frequency = 0.31 cycles/pixel, pixel size = 0.53 cm for our system setup). Then, the projection dataset was reconstructed over 180° (45° RAO to LPO) with filtered backprojection (ramp filter) and no attenuation correction and the transaxial images reoriented into short-axis images. Application of the quantitative gated SPECT algorithm to ungated tomographic images produces an EF = 0, but it nevertheless results in the calculation of epicardial and endocardial volumes. We applied the algorithm to the phantom images 10 times, varying between 10% and 80% the percentage of $s.d._{in}$ that determines where the epicardial boundary is located. The relative endocardial volumes were graphed and interpolated to determine the percentage of $s.d._{in}$ corresponding to the correct value of 63 ml.

After setting the percentage of $s.d._{in}$ to the value thus determined, the projection data were prefiltered with 40 different two-dimensional Butterworth filters (order = 5 and critical frequencies varying from 0.1 to 0.5 cycles/pixel in 0.01 steps) to fully encompass any filtering need required by different system resolutions and/or different counting statistics. The data were reconstructed and reoriented as previously described. Application of the quantitative gated SPECT algorithm to all datasets allowed investigation of the influence of pre-reconstruction filtering on the endocardial volumes and therefore on the ejection fractions measured.

Patient Studies: Gated Technetium-99m-Sestamibi SPECT

The quantitative algorithm was applied to short-axis images from 65 patients undergoing rest gated 99m Tc-sestamibi SPECT. The patient population comprised 45 men and 20 women with ($n = 25$) and without ($n = 40$) prior myocardial infarction. Prior infarcts were localized in the anterior myocardium ($n = 8$), the inferior myocardium ($n = 12$) or both regions ($n = 3$), with two cases undetermined. In nine patients, the infarct was large. Patient demographics are described in Table 1. All studies were acquired on the same triple-detector camera previously described 1 hr after the injection of 25–30 mCi 99m Tc-sestamibi. The camera used LEHR collimation, continuous detector rotation, 3° projections and 40 sec of data collection per projection, distributed over 16 cardiac frames. There was no bad beat rejection; i.e., the acceptance window was set at 100%. Immediately after acquisition, the 16 intervals at each projection angle were compacted into 8 (by summation of intervals 1 + 2, 3 + 4, etc.), as well as into 1 (summed or ungated projection dataset). The projection datasets were prefiltered with a two-dimensional Butterworth filter (order = 2.5 and critical frequency = 0.22 cycles/pixel for the 16- and the

8-intervals sets, 0.31 cycles/pixel for the ungated set, pixel size = 0.53 cm), reconstructed over 180° (45° RAO to LPO) with filtered backprojection (ramp filter) and no attenuation correction. The resulting transaxial image sets were reoriented into short-axis sets, after which the 16- and the 8-intervals sets were transferred to a stand-alone workstation (Sun SPARC IPX, 32 MB RAM) running the automatic ejection fraction quantification software and processed in batch mode. The ungated set was used for routine rest-perfusion assessment as part of a two-day stress/rest ^{99m}Tc-sestamibi protocol.

Patient Studies: Technetium-99m-Sestamibi Radionuclide Angiogram (RNA)

In all patients, rest-gated SPECT was preceded by rest first-pass RNA. First-pass data were collected during the 25–30 mCi ^{99m}Tc-sestamibi injection, with the patient in the upright position (anterior view). Images were obtained with a multicrystal, high count rate, small field of view gamma camera and a high sensitivity collimator. The acquisition protocol consisted of 1000 temporal frames at 25 msec/frame and a 20% window centered on the 140-keV photopeak of ^{99m}Tc. Processing utilized commercially available algorithms that sequentially performed deadtime and uniformity correction, temporal smoothing, creation of a preliminary left ventricular representative cycle, background modification and creation of a final representative cycle from which end-diastole and end-systole left ventricular regions of interest were assigned manually (37). The left ventricular ejection fraction was then calculated automatically. In this implementation of the quantitative algorithms, the position of the valve plane was assumed constant throughout the cardiac cycle.

RESULTS

Phantom Experiments

Figure 3 shows the different endocardial volumes measured by the quantitative gated SPECT algorithm in the cardiac phantom. As explained earlier, the nonuniform distance (from the midmyocardial surface) defining the endocardial surface, expressed as the percent s.d._{in} for the Gaussian fit to each count profile through the myocardium, varied from 10% to 80%. Figure 3 illustrates, as expected, that there is an inverse linear relationship ($y = 104.06 - 0.62x$, $r = 0.996$, s.e.e. = 1.61) between the percentage of s.d._{in} used and the measured endocardial volumes. The actual left ventricular cavity volume of 63 ml was measured in correspondence to 65% of s.d._{in} and, consequently, this parameter value was adopted for all subsequent analyses (phantom and clinical studies).

Figure 4 shows the endocardial volumes measured by the quantitative gated SPECT algorithm in the cardiac phantom in correspondence to 40 different pre-reconstruction smoothings of the projection data. The critical frequency of the pre-reconstruction filter (Butterworth, order = 2.5) varied from 0.1 to 0.5 cycles/pixel in 0.01 steps. Figure 4 demonstrates that volumes are within ±10% of the real value (63 ml) as long as the critical frequency of the filter is above 0.17 cycles/pixel, a value far lower than that used in clinical practice.

It is appropriate to note at this point that the validation of volumes obtained with our algorithm was not within the

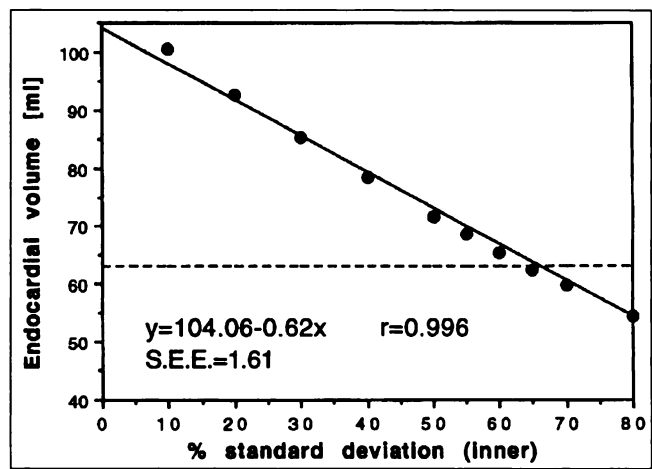


FIGURE 3. Endocardial volumes measured by the quantitative gated SPECT algorithm in a cardiac phantom as a function of the percentage of s.d._{in} chosen to represent the endocardial surface. Actual left ventricular cavity volume (63 ml) was measured in correspondence of 65% of s.d._{in}.

scope of this paper, and that the previous experiments were performed solely to fine-tune the parameters to be used in calculating LVEF. Since the ejection fraction is essentially a ratio of volumes, it is reasonable to assume that any error made in the estimation of the endocardial surface (volume) would be in the same direction at end-systole and end-diastole, and therefore would be at least partially canceled out during the derivation of the ejection fraction.

Clinical Studies

Segmentation and contouring of the LV was successful in 65/65 (100%) of the studies. Success is defined as the selection of slices and generation of endocardial and epicardial contours that match the contours visually apparent in the images. An example of the algorithm's output is

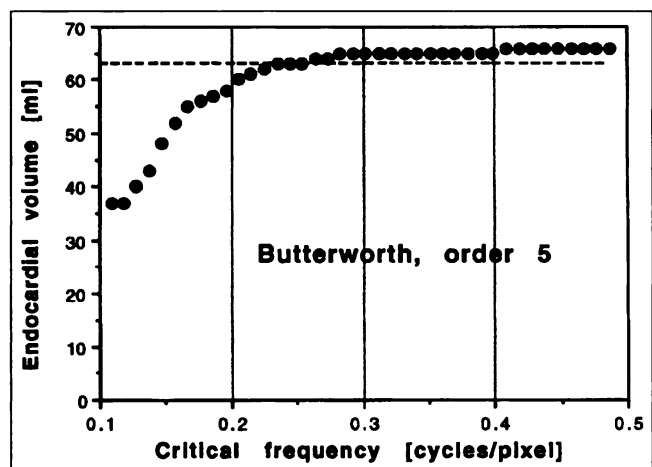


FIGURE 4. Endocardial volumes measured by the quantitative gated SPECT algorithm in the cardiac phantom, in correspondence to 40 different pre-reconstruction smoothings of the projection data. Volumes are within ±10% of the real value (63 ml) as long as the critical frequency of the order 2.5 Butterworth filter is above 0.17 cycles/pixel, a value far lower than that used in clinical practice.

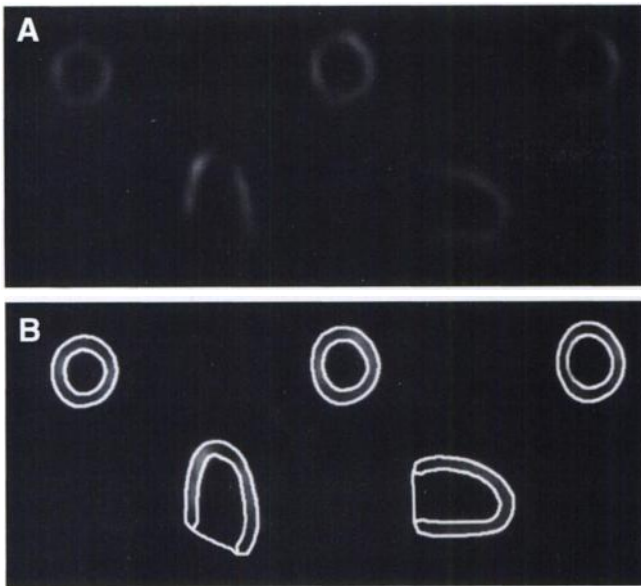


FIGURE 5. Myocardial contours overlaid by the quantitative gated SPECT algorithm onto three short-axis (top row, left to right = apical, mid and basal) images, a midhorizontal and a midvertical long-axis image (bottom row) of a normal patient at end-diastole. Contour display provides visual evaluation of the algorithm's successful completion. Images corresponding to any of the 8 or 16 gating intervals can be displayed, or cine looping throughout all intervals can be performed in real time.

shown in Figure 5, which displays three short-axis (top row, left to right = apical to basal), a horizontal and a vertical long-axis image (bottom row) for a normal patient at end-diastole, with endocardial and epicardial contours superimposed onto all images. We have developed a display of apical, mid and basal short-axis slices and midventricular vertical long-axis and horizontal long-axis slices as the automatic default of the algorithm. If segmentation should fail, the software enable manual definition of a three-dimensional mask encompassing the left ventricle, so that the

algorithm would only operate within the mask's domain. In addition to the two-dimensional slice display of Figure 5, the software provides for three-dimensional display of the epicardial and endocardial surfaces (Fig. 6). Both the slice and the surface display can present the images in cinematic fashion, endlessly looping through the eight gating intervals at a user-determined speed. This allows visual evaluation of wall motion and thickening to be employed in conjunction with automated techniques under development at this laboratory. An example of the final report is displayed in Figure 7. The endocardial volume curve as a function of the gating interval is accompanied by patient data along with the measured global ejection fraction value and a synthetic comparison of the five images in Figure 5 at end-diastole and end-systole. Figures 5–7 refer to the same normal patient, with an ejection fraction of 64%. Figure 8 demonstrates how, in a patient with coronary artery disease, the algorithm returns visually correct contours even when large and severe perfusion defects are present. This patient had severe and extensive anterior and apical perfusion defects and a global ejection fraction of 20% (Fig. 9).

Figure 10 plots the 8-interval ejection fractions versus the 16-interval ejection fractions, as measured by the quantitative gated SPECT algorithm, in all 65 clinical patients. The two sets show high linear agreement ($y = -2.7 + 0.97x$, $r = 0.988$, $p < 0.001$, $s.e.e. = 2.65$). As expected, compacting the 16-interval datasets into 8 intervals leads to lower ejection fractions, because this is equivalent to smoothing the time-volume curve. The Bland-Altman plot in Figure 11 expresses the absolute reduction in ejection fraction as a function of the measured ejection fraction (averaged between 16 and 8 intervals) and demonstrates that no relevant trend exists over a wide ejection fraction range. The average reduction in ejection fraction by using 8-interval gating is 3.71 percentage points.

Figure 12 shows the relationship between the 8-interval

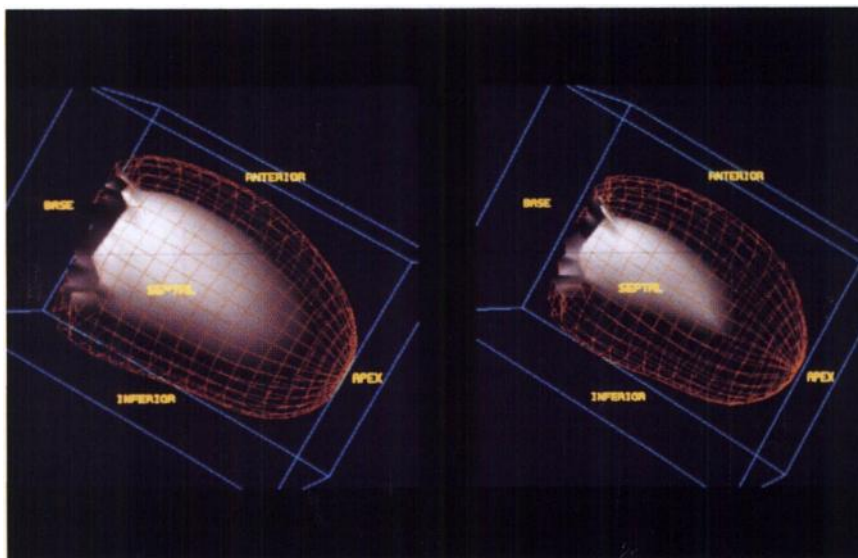


FIGURE 6. Three-dimensional display of the endocardial (solid) and epicardial (grid) surfaces calculated by the automatic algorithm for the same patient in Figure 5 at end-diastole (left) and end-systole (right).

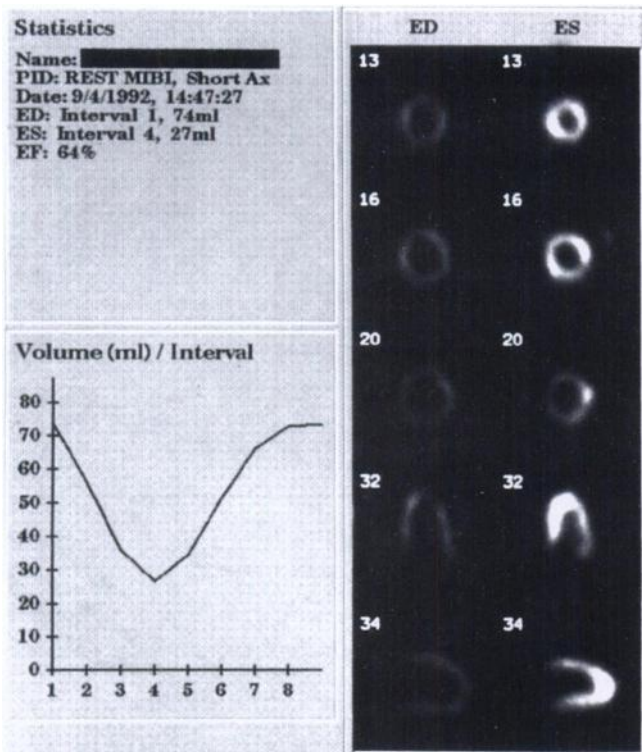


FIGURE 7. Quantitative gated SPECT algorithm results for the patient in Figures 5 and 6. The endocardial time-volume curve is displayed and the global LVEF (64%) is calculated and reported along with patient data and representative short- and long-axis images at end-diastole and end-systole.

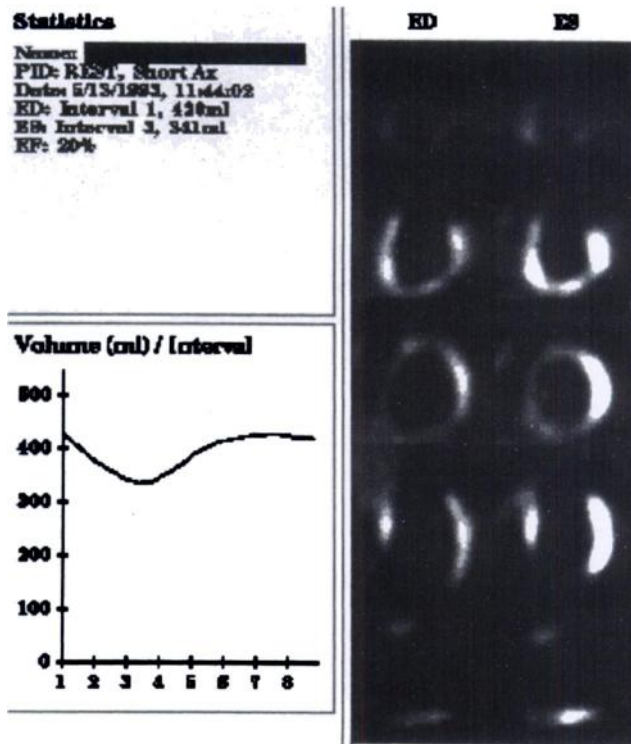


FIGURE 9. Quantitative gated SPECT algorithm results for the patient in Figure 8. Global LVEF (20%) and dynamic range of the endocardial time-volume curve are lower compared to the normal patient in Figure 7.

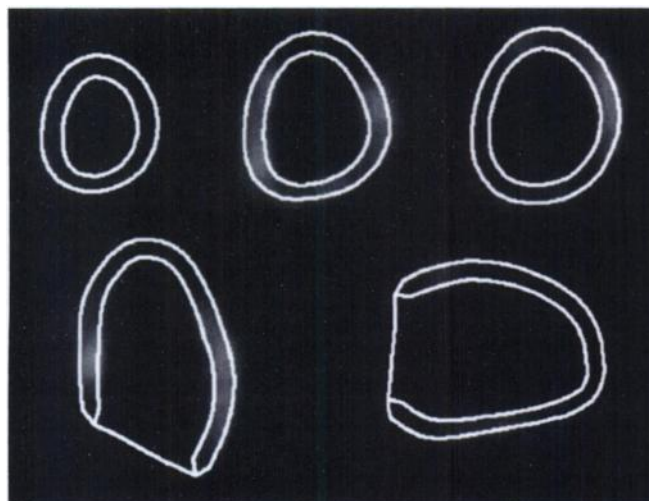


FIGURE 8. Myocardial contours overlaid by the quantitative gated SPECT algorithm onto the end-diastolic, short-axis (top row) and long-axis images of a patient with severe and extensive anterior and apical perfusion defects. Contours are generated even in the apparent absence of perfusion by using smoothing, the isocontours of the coordinate system and the geometry of the defect boundaries as constraints. Zoom is the same as in Figure 5, suggesting a larger heart for this patient compared to the patient in Figure 5.

ejection fraction measured by the automatic algorithm on the gated SPECT images and the first-pass ejection fractions. The two sets show high linear agreement ($y = 2.44 + 1.03x$, $r = 0.909$, $p < 0.001$, $s.e.e. = 6.87$), with the gated SPECT derived ejection fractions being slightly higher than the first-pass ejection fractions on average. If 8-interval gated SPECT further underestimates measured ejection

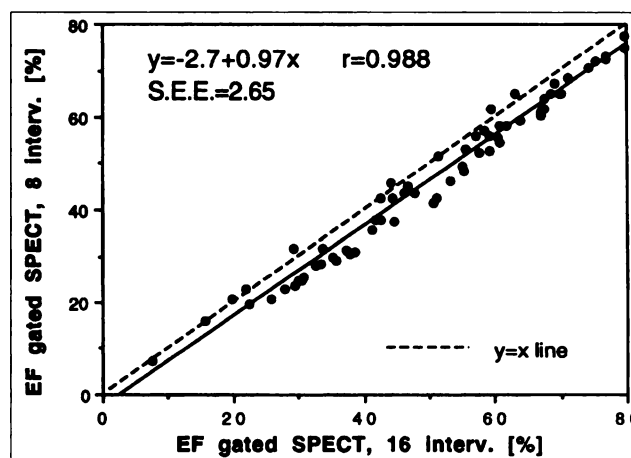


FIGURE 10. Comparison between 16-interval and 8-interval ejection fractions. Reducing the number of gating intervals results in lower ejection fractions, but the linear agreement between ejection fraction values for these two gating strategies is excellent ($r = 0.988$).

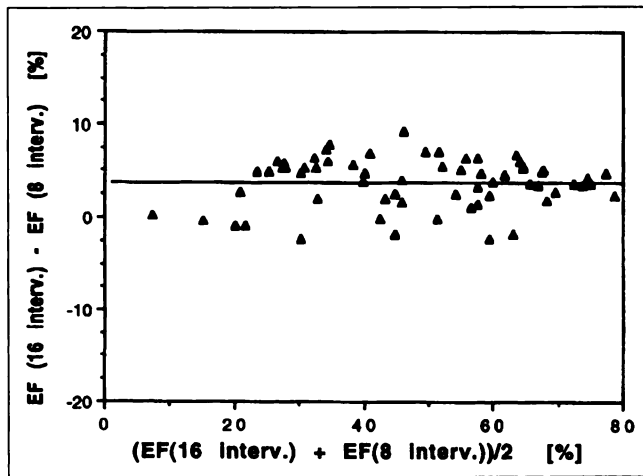


FIGURE 11. Bland-Altman plot shows the absolute difference between ejection fraction values measured from 16-interval and 8-interval gated data. The average reduction in ejection fraction by using 8-interval gating is 3.71 percentage points, with no apparent trend over a wide range of ejection fractions.

fractions compared to 16-interval gating, then gated SPECT ejection fractions are measured as being approximately 10% greater than first-pass ejection fractions. This bias would likely be compensated by abandoning the constraint of a fixed valve plane in the first-pass ejection fraction calculation, as confirmed by preliminary results from our laboratory.

DISCUSSION

There are several perceived impediments to the wide diffusion of gated SPECT in clinical nuclear cardiology. The major concerns are the length of the gated acquisition, the large body of data generated and the lack of automated methods for quantification of functional parameters such as LVEF.

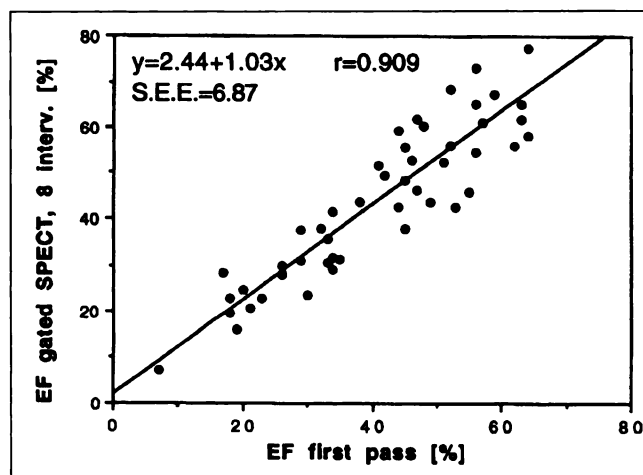


FIGURE 12. Relationship between 8-interval ejection fractions measured by the automatic quantitative gated SPECT algorithm and first-pass ejection fractions. Note the high linear agreement ($r = 0.909$) between the two sets of values.

Gated SPECT Acquisition Duration

It is commonly believed that the duration of a gated SPECT acquisition must be longer than that of a standard SPECT acquisition since the counts generated by the same injected dose must be distributed over 8 or 16 image sets. In this view, the lower the number of intervals the better the statistical quality of each image set, and therefore the shorter the global acquisition time required. One of the goals of this study has been to prove that although the use of 8 gating intervals somewhat depresses ejection fraction values, compared to 16 intervals, this decrease is predictable and, in fact, essentially constant over a wide range of ejection fractions, so that the appropriate corrections can be readily implemented. Consequently, we can now recommend on quantitative grounds the use of 8-interval gated myocardial perfusion SPECT, which is already generally preferred to 16-interval gating. A more provocative thought is that it is not truly necessary for gated acquisition to be longer than standard nongated acquisition. The perfusion data derived from a summed gated SPECT study is the same as that from a standard SPECT study of the same duration if, as in our protocol, no data are rejected because of irregular cardiac beats. Functional parameters are measured from individual intervals' images, and would be expected to be affected most by shorter acquisitions. Preliminary results from our laboratory, however, indicate that fast (6.7 min) gated SPECT, in conjunction with our automated quantification software, produces quantitative ejection fraction values that agree extremely well with those from standard gated SPECT and that visual determinations of wall motion and thickening are virtually identical between fast and standard gated SPECT (38). It is conceivable that the total duration of gated SPECT studies could be shorter than that currently used for standard SPECT studies and this may encourage future investigation in the routine gating of ^{201}Tl SPECT studies. A key factor in reducing the duration of gated SPECT studies will be the performance of such acquisition in conjunction with continuous detector rotation so as to eliminate the deadtime intrinsic to the step-and-shoot technique (39).

Storage of Gated SPECT Datasets

The dimension of gated SPECT studies is substantially greater (by a factor roughly equal to the number of intervals used) compared to regular SPECT. This is, however, a situation analogous to the acquisition of dynamic (sequential) SPECT studies using $^{99\text{m}}\text{Tc}$ -teboroxime, or of dynamic PET studies using ^{13}N , ^{11}C , ^{15}O or ^{82}Rb . A possible strategy to minimize storage and archival requirements is to save only the projection data (~4 Mbytes for 60 projections) and the short-axis data (~2 Mbytes for 30 slices), discarding filtered projections, transaxial images and reoriented long-axis images immediately after reconstruction. If desired, compression of the data can be implemented using standard techniques. Compression will likely be preferred in teleradiology applications involving rapid transfer of gated SPECT data, although the most popular image format in

nuclear medicine does not handle four-dimensional data structures yet (40).

Are Planar Techniques an Adequate Gold Standard for Ejection Fraction Measurement?

We have described our development of automated tools to allow quantification of LVEF from gated SPECT studies. Previous approaches to this problem had been either subjective (15) or partially automatic (10,29). We have validated the ejection fractions calculated by our automated algorithm against those calculated from planar first-pass RNA. Although the agreement between the two techniques is high ($r = 0.909$), there is reason to believe that the first-pass RNA gold standard may be inferior to this quantitative gated SPECT technique. Limitations of the planar technique include manual region of interest drawing and uncertainty regarding the valve plane location. Moreover, when geometric methods for estimating endocardial volume are applied to two-dimensional images, assumptions must be made as to the shape of the left ventricular cavity. The left ventricular cavity is usually assumed to have the shape of an ellipsoid or a prolate spheroid, and its volume is estimated from its area and long-axis in the specific projection acquired (21,23–24). To the extent that the left ventricle deviates from the postulated model, the results will be incorrect (41). The error in determining end-diastolic and end-systolic volumes is propagated in the computation of the ejection fraction, resulting in larger errors for this derived quantity. The accuracy of count-based methods to estimate left ventricular cavity volumes from planar images is also far from high (42–43). One advantage the first-pass technique has over gated SPECT is the greatly reduced influence of partial volume effects due to the fact that the left ventricular cavity has a diameter larger than the myocardial wall thickness (44). The modeling and compensation of partial volume effects in the estimation of myocardial wall thickness from gated tomographic data, however, is possible, as demonstrated by other investigators (45). We have shown that our choice of the endocardial surface is relatively independent of the level of pre-reconstruction image filtering or the statistical quality of the data. Even if systematic errors in border estimation occurred due to imperfect handling of the partial volume effect, these errors would similarly affect the end-diastolic and the end-systolic volume and, thus, at least partially cancel each other in calculating ejection fraction values. In another example of volume ratios, application of the method described in this article to calculate the ratio of stress-to-rest endocardial volumes in nongated SPECT has proven effective in measuring transient ischemic dilation of the left ventricle (46), a marker of severe and extensive coronary artery disease (47).

Future Directions

Future extensions of our automated, quantitative gated SPECT algorithm will involve validating the endocardial volumes (not just their derived quantity, ejection fraction) using gated cardiac MRI. In addition, measurement, vali-

dation and display of regional motion, thickening and ejection fraction data will have to be obtained from a large population of patients. Once this is done, the generation of normal limits for regional functional parameters can be implemented, as is already available for perfusion data (48), and parametric polar maps combining perfusion and function information can be developed.

CONCLUSION

We have developed a completely automatic algorithm to measure quantitatively LVEFs from gated ^{99m}Tc -sestamibi myocardial perfusion SPECT. The algorithm was applied successfully to 100% of 65 clinical patient studies acquired with 16- and 8-interval gating, was perfectly reproducible and produced results in good agreement with first-pass RNA data. The automatic ejection fraction quantification algorithm consists of three steps: segmenting the left ventricular myocardium, extracting the left ventricle's midmyocardial surface and determining the endocardial and epicardial surfaces based on asymmetric Gaussian fitting of the count profiles across the midmyocardial surface. In its current implementation on a relatively inexpensive (<\$5000) off-the-shelf computer, the algorithm is fast, portable and does not require any proprietary hardware or special pre-processing. Quantitative measurement of LVEF from gated myocardial perfusion SPECT may provide a catalyst for the clinical diffusion of gated SPECT protocols.

ACKNOWLEDGMENTS

The authors thank Dr. Erik Alexanderson, Art Cabico, Gerry Fernandez, Mark Hyun and Ponce Tapnio for their technical assistance. This work was supported in part by a Whitaker Foundation Biomedical Engineering Research grant.

REFERENCES

1. Berman D. Technetium-99m myocardial perfusion imaging agents and their relation to thallium-201. *Am J Cardiol* 1990;66:1E–4E.
2. Maddahi J, Kiat H, Van Train K, et al. Myocardial perfusion imaging with technetium-99m sestamibi SPECT in the evaluation of coronary artery disease. *Am J Cardiol* 1990;66:55E–62E.
3. Najm Y, Timmis A, Maisey M, et al. The evaluation of ventricular function using gated myocardial imaging with ^{99m}Tc MIBI. *Eur Heart J* 1989;10:142–148.
4. Mannting F, Morgan-Mannting M. Gated SPECT with technetium-99m sestamibi for assessment of myocardial perfusion abnormalities. *J Nucl Med* 1993;34:601–608.
5. Eisner R, Schmarkey L, Martin S, et al. Defects on SPECT perfusion images can occur due to abnormal segmental contraction. *J Nucl Med* 1994;35:638–643.
6. Chua T, Kiat H, Germano G, et al. Gated technetium-99m sestamibi for simultaneous assessment of stress myocardial perfusion, post-exercise regional ventricular function and myocardial viability: correlation with echocardiography and rest thallium-201 scintigraphy. *J Am Coll Cardiol* 1994;23:1107–1114.
7. Grucker D, Florentz P, Ozwald T, Chambron J. Myocardial gated tomoscintigraphy with ^{99m}Tc -methoxy isobutyl isonitrile (MIBI): regional and temporal activity curve analysis. *Nucl Med Commun* 1989;10:723–732.
8. Marcassa C, Marzullo P, Parodi O, Sambuceti G, L'Abbate A. A new method for noninvasive quantification of segmental myocardial wall thickening using ^{99m}Tc -2-methoxy-isobutyl-isonitrile scintigraphy—results in normal subjects. *J Nucl Med* 1990;31:173–177.
9. Galt J, Garcia E, Robbins W. Effects of myocardial wall thickness on SPECT quantification. *IEEE Trans Med Imag* 1990;9:144–150.
10. Faber T, Akers M, Pesnock R, Corbett J. Three-dimensional motion and

- perfusion quantification in gated single-photon emission computed tomograms. *J Nucl Med* 1991;32:2311-2317.
11. Cooke C, Garcia E, Cullom S, Faber T, Pettigrew R. Determining the accuracy of calculating systolic wall thickening using a fast Fourier transform approximation: a simulation study based on canine and patient data. *J Nucl Med* 1994;35:1185-1192.
 12. Yamashita K, Tamaki N, Yonekura Y, et al. Quantitative analysis of regional wall motion by gated myocardial positron emission tomography: validation and comparison with left ventriculography. *J Nucl Med* 1989;30:1775-1786.
 13. Yamashita K, Tamaki N, Yonekura Y, et al. Regional wall thickening of left ventricle evaluated by gated PET in relation to myocardial perfusion and glucose metabolism. *J Nucl Med* 1991;32:679-685.
 14. Berman D, Kiat H, Van Train K, et al. Myocardial perfusion with technetium-99m-sestamibi: comparative analysis of available imaging protocols. *J Nucl Med* 1994;35:681-688.
 15. DePuey E, Nichols K, Dobrinsky C. Left ventricular ejection fraction assessed from gated technetium-99m-sestamibi SPECT. *J Nucl Med* 1993;34:1871-1876.
 16. Shah P, Pichler M, Berman D, Singh B, Swan H. Left ventricular ejection fraction determined by radionuclide ventriculography in early stages of first transmural myocardial infarction. *Am J Cardiol* 1980;45:542-546.
 17. European Coronary Surgery Study Group. Long-term results of prospective randomised study of coronary artery bypass surgery in stable angina pectoris. *Lancet* 1982;2(8309):1173-1180.
 18. Coronary artery surgery study (CASS): a randomized trial of coronary artery bypass surgery. Survival data. *Circulation* 1983;68:939-950.
 19. Risk stratification and survival after myocardial infarction. *N Engl J Med* 1983;309:331-336.
 20. Lee K, Pryor D, Pieper K, et al. Prognostic value of radionuclide angiography in medically treated patients with coronary artery disease. A comparison of clinical and catheterization variables. *Circulation* 1990;82:1705-1717.
 21. Strauss H, Zaret B, Hurley P, Natarajan T, Pitt B. A scintiphotographic method for measuring left ventricular ejection fraction in man without cardiac catheterization. *Am J Cardiol* 1971;28:575-580.
 22. Berman D, Salel A, DeNardo G, Bogren H, Mason D. Clinical assessment of left ventricular regional contraction patterns and ejection fraction by high-resolution gated scintigraphy. *J Nucl Med* 1974;16:865-874.
 23. Uren R, Newman H, Hutton B, et al. Geometric determination of left ventricular volume from gated blood-pool studies using a slant-hole collimator. *Radiology* 1983;147:541-545.
 24. DePuey E. Evaluation of cardiac function with radionuclides. In: H. a. P. Gottschalk, eds. *Diagnostic nuclear medicine*, 2nd ed. Baltimore: Williams & Wilkins; 1988:355-398.
 25. Barat J, Brendel A, Colle J, et al. Quantitative analysis of left-ventricular function using gated single photon emission tomography. *J Nucl Med* 1984;25:1167-1174.
 26. Caputo G, Graham M, Brust K, Kennedy J, Nelp W. Measurement of left ventricular volume using SPECT. *Am J Cardiol* 1985;56:781-786.
 27. Gill J, Moore R, Tamaki N, et al. Multigated blood-pool tomography: new method for the assessment of left ventricular function. *J Nucl Med* 1986;12:1916-1924.
 28. Yamashita K, Tanaka M, Asada N, et al. A new method of three-dimensional analysis of left ventricular wall motion. *Eur J Nucl Med* 1988;14:113-119.
 29. Nuyts J, Suetens P, Oosterlinck A, De Roo M, Mortelmans L. Delineation of ECT images using global constraints and dynamic programming. *IEEE Trans Med Imag* 1991;10:489-498.
 30. Zucker S, Hummel R, Rosenfeld A. An application of relaxation labeling to line and curve enhancement. *IEEE Trans Comput* 1977;C-26:394-403.
 31. Richards J, Landgrebe D, Swain P. On the accuracy of pixel relaxation labeling. *IEEE Trans Syst Man Cybernet* 1981;SMC-11:303-309.
 32. Winston P. *Artificial intelligence*, 3rd ed. Reading, MA: Addison-Wesley; 1992.
 33. Ballard D, Brown C. *Computer vision*. Englewood Cliffs, NJ: Prentice-Hall; 1982.
 34. Germano G, Kavanagh P, Su H, et al. Automatic reorientation of three-dimensional, transaxial myocardial perfusion SPECT images. *J Nucl Med* 1995;36:1107-1119.
 35. Ratib O, Huang H. CALIPSO: an interactive software package for multi-modal medical image analysis on a personal computer. *J Med Imaging* 1989;3:205-216.
 36. Hoffman E, Huang S, Phelps M. Quantitation in PET. I. Effect of object size. *J Comput Assist Tomogr* 1979;3:299-308.
 37. Friedman J, Berman D, Kiat H, et al. Rest and treadmill exercise first-pass radionuclide ventriculography: validation of left ventricular ejection fraction measurements. *J Nucl Cardiol* 1994;1:382-388.
 38. Mazzanti M, Kiat H, Germano G, Friedman J, Berman D. Fast ^{99m}Tc sestamibi gated SPECT for the evaluation of myocardial function [Abstract]. *Circulation* 1994;90:1-11.
 39. Germano G, Kavanagh P, Kiat H, Van Train K, Berman D. Temporal image fractionation: rejection of motion artifacts in myocardial SPECT. *J Nucl Med* 1994;35:1193-1197.
 40. Todd-Pokropek A, Craddock T, Deconinck F. A file format for the exchange of nuclear medicine data: a specification of Interfile version 3.3. *Nucl Med Commun* 1992;13:673-699.
 41. Slutsky R, Karlner J, Ricci D, et al. Left ventricular volumes by gated equilibrium radionuclide angiography: a new method. *Circulation* 1979;60:556-564.
 42. Levy W, Cerqueira M, Matsuoka D, et al. Four radionuclide methods for left ventricular volume determination: comparison of a manual and an automated technique. *J Nucl Med* 1992;33:763-770.
 43. Levy W, Jacobson A, Cerqueira M, et al. Radionuclide cardiac volumes: effects of ROI selection and correction for Compton scatter using a buildup factor. *J Nucl Med* 1992;33:1642-1647.
 44. Gambhir S, Huang S, Digby W, Schelbert H, Phelps M. A new method for partial volume and spillover correction in cardiac PET scans. *J Nucl Med* 1989;30:824-825.
 45. Gambhir S. *Quantitation of the physical factors affecting the tracer kinetic modeling of cardiac PET data*. PhD dissertation; University of California, Los Angeles, 1990.
 46. Mazzanti M, Germano G, Kiat H, et al. Identification of severe and extensive coronary artery disease by automatic measurement of transient ischemic dilation in dual isotope myocardial perfusion SPECT [Abstract]. *Circulation* 1994;90:1-448.
 47. Weiss A, Berman D, Lew A, et al. Transient ischemic dilation of the left ventricle on stress thallium-201 scintigraphy: a marker of severe and extensive coronary artery disease. *J Am Coll Cardiol* 1987;9:752-759.
 48. Van Train K, Areeda J, Garcia E, et al. Quantitative same-day rest-stress technetium-99m-sestamibi SPECT: definition and validation of stress normal limits and criteria for abnormality. *J Nucl Med* 1993;34:1494-1502.